Influence of humidified aerosol on lidar depolarization measurements below ice-precipitating Arctic stratus

Bastiaan van Diedenhoven *

Columbia University, Center for Climate System Research, New York, NY

Ann M. Fridlind

Andrew S. Ackerman

NASA Goddard Institute for Space Studies, New York, NY

* *Corresponding author address:* Bastiaan van Diedenhoven, 2880 Broadway, New York, NY 10025, USA

E-mail: bvandiedenhoven@giss.nasa.gov

ABSTRACT

Lidar measurements obtained during the Surface Heat Budget of the Arctic Ocean (SHEBA) experiment under a mixed-phase stratus cloud that was lightly precipitating ice show a range of surprisingly low depolarization ratios (4–23%), despite an absence of cloud droplets. These depolarization ratios are much lower than the range of theoretical values obtained for various ice habits. The depolarization ratios correlate well with radar reflectivity, suggesting that the variation in depolarization ratios results from variations in ice water content, rather than variation in ice habits or orientation. By calculating lidar depolarization based on (i) large-eddy simulations and (ii) *in situ* ice size distribution measurements, we show that the presence of humidified aerosol particles in addition to the ice precipitation can explain the distribution of the observed depolarization ratios, although uncertainties related to the aerosol size distributions are substantial. These calculations show that humidified aerosol must be taken into account when interpreting lidar depolarization measurements for cloud and precipitation phase discrimination or ice habit classification, at least under conditions similar to those observed during SHEBA.

1. Introduction

Lidar measurements can provide a wealth of information about macro- and microphysical properties of aerosols and clouds (Weitkamp 2005). In particular, lidars that emit circularly or linearly polarized light and measure the depolarization of the returned signal have proven to be very useful in the study of clouds. For instance, lidar depolarization measurements can be used to study and classify ice crystals in clouds and precipitation, since depolarization

properties depend on microphysical properties of the ice crystals such as habit, aspect ratio and crystal orientation (Noel et al. 2002; Del Guasta et al. 2006; You et al. 2006). Depolarization measurements can also be used to distinguish ice from liquid particles since light scattered from non-spherical ice particles is depolarized whereas light scattered from spherical drops is not (Shupe et al. 2005; de Boer et al. 2011). Generally, linear depolarization ratios below about 10–15% are considered to indicate liquid, while higher depolarizations point to the presence of ice crystals (Sassen et al. 1992; Intrieri et al. 2002). Some more advanced schemes use other measurements in addition to lidar depolarization to classify cloud phase, such as lidar backscatter coefficients, radar reflectivity and Doppler velocity, but lidar depolarization serves as a critical parameter in these schemes (Shupe et al. 2005; Shupe 2007; Bourdages et al. 2009). In mixed-phase conditions, depolarization ratio measurements also can provide information about the relative concentrations of non-spherical ice and liquid drops (van Diedenhoven et al. 2009; Bourdages et al. 2009). For example, van Diedenhoven et al. (2009) evaluated simulations of a mixed-phase stratocumulus cloud observed during the Mixed-phase Arctic Cloud Experiment (M-PACE) by comparing simulated and observed distributions of lidar backscatter, radar reflectivity and radar Doppler velocity, in addition to distributions of circular depolarization ratios below cloud, measured to be between 0 and 200% (corresponding to linear depolarizations from 0% to ∼50% (Mishchenko and Hovenier 1995)). Only simulations with sufficiently rapid glaciation of mixed-phase precipitation (drizzle and ice) below cloud base were found to reproduce all radar and lidar metrics, including lidar depolarization. However, the impact of aerosol on depolarization was neglected in that study.

In this paper, we focus on linear depolarization measurements by the Depolarization and

Backscatter Unattended Lidar (DABUL) under a mixed-phase stratus cloud observed during Surface Heat Budget of the Arctic Ocean (SHEBA) experiment (Uttal et al. 2002) over the last 12 hours of 7 May, 1998 (Zuidema et al. 2005). Figure 1 shows a time series of the measured lidar depolarization below cloud base. Measurements show linear depolarization ratios below cloud base ranging from 4 to 23%. Statistics presented by Intrieri et al. (2002) show that such low depolarization values were very commonly measured at low altitudes during the SHEBA campaign. These depolarization ratios are below the range of theoretical values associated with different ice habits, which typically vary from 25–70% (Sassen et al. 1992; Del Guasta et al. 2006; You et al. 2006), and are often below the limit of 10–15% assumed to indicate liquid cloud particles. Furthermore, Fig. 1 shows that the depolarization ratios correlate well with the radar reflectivities under cloud measured by the Millimeter Cloud Radar (MMCR; Moran et al. 1998), with a correlation coefficient of 0.77. Considering radar reflectivity as a proxy for ice water content (Shupe et al. 2005), this correlation strongly suggests that changes in depolarization are associated with changes in ice water contents, rather than ice habit or aspect ratio variations or variations in ice orientation. However, as the observed cloud during SHEBA has a relatively low liquid water path and high droplet concentration, no liquid droplets are expected below cloud base (Comstock et al. 2004; Zuidema et al. 2005) to explain the low depolarization values in the regions with low ice concentrations. Also, in contrast to the M-PACE case study, no liquid precipitation was observed in CPI images taken below cloud base (Zuidema et al. 2005). As hypothesized by Zuidema et al. (2005), these low depolarization values hint at the presence of humidified aerosol under cloud base. It was noted previously by Sassen et al. (1992) that the depolarization in the snowfall region below cloud base could be appreciably influenced by growing haze particles. In this study we

use calculations of depolarization ratios based on large-eddy simulations (LES) and *in situ* measurements to show that these low lidar depolarization ratios indeed can be explained by the presence of humidified aerosol particles amid ice precipitation, and that humidified aerosol should be considered when interpreting lidar depolarization measurements for cloud and precipitation phase discrimination and ice habit classification.

After describing the data in section 2 and simulations in section 3, we present results in section 4 and conclusions in section 5.

2. Measurements

As part of the SHEBA campaign, the DABUL lidar was deployed on an icebreaker ship frozen into the winter ice pack of the Beaufort Sea (Intrieri et al. 2002). DABUL operates at 532 μm and transmits linearly polarized light, which enables the measurement of depolarization ratios with a vertical resolution of 30 m and a temporal resolution of 10 seconds. The field-of-view of the DABUL measurements used here is 100 μrad. Although DABUL was not well calibrated during SHEBA, calibration errors are expected to largely cancel out for the depolarization ratios. The lidar was tilted 5° off zenith to avoid specular reflection from oriented plates that result in near zero depolarization values (Intrieri et al. 2002).

The observed cloud base was steady around 280 m throughout the last 12 hours UTC of May 7th, 1998, while cloud top height gradually fell from about 600 m at midday to around 400 m at the end of the day (Shupe et al. 2006; Fridlind et al. 2011). Cloud temperatures were roughly in the range of -16° to -20° C.

Unfortunately no aerosol size or composition measurements are available for SHEBA. Following Morrison et al. (2011), here we base the dry aerosol size distributions on those derived from measurements during M-PACE with the total concentration in the fine mode increased to reflect the more polluted conditions during SHEBA. Figure 2 shows particle concentrations measured in the 5 smallest size bins of the Met One Handheld Particle Counter (HHPC-6) flown on an Aerosonde UAV on 10 October during M-PACE. Only HHPC-6 measurements below cloud base with an ambient relative humidity (RH) below 70% are considered here, since significant spurious high concentrations of particles in the largest bins are seen for higher RH. (For example, the inter-quartile range (IQR) of concentration in the 2–5 μm channel is 0.45 when all measurements are included and 0.09 when only measurements with RH<70% are included.) A six-parameter bimodal log-normal size distribution (geometric mean radius r_m, geometric standard deviation σ_g, and total number concentration N in each mode) was numerically fit through the median values of the HHPC-6 measurements (see Fig. 2). The fit parameters are listed in Table 1. To reflect the more polluted conditions during SHEBA relative to the M-PACE case, the number concentration in the fine mode was increased to 350 cm^{-3}, following Morrison et al. (2011). Figure 2 also includes the fit presented by Morrison et al. (2008), which differs significantly from ours, primarily in the coarse mode. This difference occurs mainly because Morrison et al. (2008) included HHPC-6 measurements at all RH and computed a fit through the mean values of the measurements as opposed to median values (the populations- of counts within each channel are highly skewed). Morrison et al. (2008) focused their analysis on characterization of the fine mode, which is most important for constraining droplet activation, while characterization of the coarse mode is more important for lidar depolarization calculations since total scattering

cross section is dominated by the coarse mode.

However, there is a substantial uncertainty associated with the derived aerosol size distributions. For example, the integrated cross-sectional area of possible fits through the IQR of the measurements in the 5 bins spans more than a factor of 150. Furthermore, the increase of number concentration in the accumulation mode for characterization of more polluted aerosol conditions during SHEBA is poorly constrained. Moreover, the SHEBA measurements were obtained over frozen ice pack, while the airmass sampled during M-PACE came from open ocean, probably leading to an increased coarse mode from sea salt. To account for the expected absence of sea salt for the SHEBA conditions, we also include lidar depolarization calculations based on the aerosol parameters with a decreased number concentration in the coarse mode.

In addition to lidar depolarization calculations based on LES, we also present lidar calculations based on *in situ* measured ice size distributions below cloud base. For this we use measurements obtained under cloud base between 22:30 and 23:00 UTC by the Forward Scattering Spectrometer Probe (FSSP; 0–53 μm maximum particle dimension) and 2-Dimensional Cloud probe (2DC; >62.5 μm) mounted on the National Center for Atmospheric Research C-130 aircraft (Zuidema et al. 2005; Fridlind et al. 2011). Such measurements are known to suffer from ice crystal shattering on the probe tips, leading to a significant overestimation of number concentration especially for ice particles with dimensions smaller than about 200 μm (Korolev and Isaac 2005; Korolev et al. 2011). To consider this effect, we also calculate lidar depolarization measurements based on the *in situ* size distribution in which crystals with maximum dimensions larger than 200 μm have been removed.

3. Simulations

The large-eddy simulations are made using the Distributed Hydrodynamic Aerosol-Radiation-Modeling Application (DHARMA) code (Stevens et al. 2002; Ackerman et al. 2003; Fridlind et al. 2011), which couples models of fluid dynamics, radiative transfer, and size-resolved, mixed-phase cloud microphysics. The DHARMA simulations represent the cloud observed in last two hours of the SHEBA case study. Three time slices output during the last hour of the simulation are randomly sampled to obtain the same number of data points as in the measurements (cf. van Diedenhoven et al. 2009). The simulations are described in detail by Fridlind et al. (2011), and are based on the SHEBA modeling intercomparison study (Morrison et al. 2011). In the present study, we use a simulation described by Fridlind et al. (2011) that uses a prognostic approach to represent heterogeneous IN activation, thus accounting for IN sources, sinks, and transport (Fridlind et al. 2007), and with IN concentration increased by a factor of 30 relative to the IN measurements above cloud. We note that it has often been found that measured IN concentrations are insufficient to explain ice in mixed-phase clouds, although myriad uncertainties remain (Beard 1992; Fridlind et al. 2007; Morrison et al. 2008; Fan et al. 2009; van Diedenhoven et al. 2009). What is important for the purposes of this study is that the simulation used here reproduces average measured radar reflectivities and *in situ* measurements of ice crystal size distributions ($D > 200$ μm) quite well (Fridlind et al. 2011).

Lidar depolarization measurements are calculated from the DHARMA model results as described by van Diedenhoven et al. (2009), but for linearly rather than circularly polarized light. Furthermore, humidified aerosol are also included in the lidar calculations in the

present study. Humidified aerosol particles are assumed to be spherical and therefore non-depolarizing. The scattering properties for humidified aerosol are calculated using Lorenz-Mie theory (Weitkamp 2005). Scattering properties of the ice are calculated using the same assumptions of projected area and aspect ratio as made in the DHARMA microphysics treatment, which is described in detail by Fridlind et al. (2011). In brief, the relation between projected area (A_p) and maximum dimension (D) corresponding to radiating assemblages of plates (Mitchell 1996) is assumed ($A_p = 0.2285\ D^{1.88}$ in cgs units). Using the mass-dimension relationships corresponding to this habit leads to the best agreement between measured radar reflectivities and the corresponding simulated values based on *in situ* measured ice size distributions; radiating assemblages of plates also agree well with CPI images obtained during the size distribution measurements (Fridlind et al. 2011). The aspect ratios are assumed to decrease linearly from 1.0 to 0.6 over a maximum dimension range of 5–120 μm, and to remain constant for larger sizes (cf. Korolev and Isaac 2003).

The optical properties are calculated using geometric optics (Macke et al. 1996), assuming the geometry of single, moderately roughened hexagonal plates with the projected areas and aspect ratios defined above. The ice crystals are assumed to be randomly oriented. Single hexagonal components of ice crystals have been shown to have similar optical properties as assemblages or aggregates of such components (Um and McFarquhar 2009; van Diedenhoven et al. 2011). Thus, the calculated optical properties are expected to represent the assumed assemblages of plates well. Depolarization ratios from backscattering off the assumed plates are about 40%, in agreement with values reported elsewhere (e.g., You et al. 2006; Noel et al. 2006; Yang and Fu 2009).

Size distributions of the humidified aerosol are derived from the dry aerosol by numeri-

cally inverting the Köhler equation using the grid-scale relative humidities produced by the DHARMA model, and assuming a constant total number concentration of aerosol below cloud base, consistent with a well-mixed boundary-layer aerosol. The aerosol is assumed to be ammonium bisulfate (Leck et al. 2002).

4. Results

Histograms of measured and simulated lidar depolarization under cloud base (60–120 m) for the last 2 hours of the 7 May SHEBA case are shown in Fig. 3. Measured median depolarization is 9.4%, with an inter-quartile range of 7.8%. As expected, when no aerosol is included in the lidar simulations, calculated median depolarizations are much too high (42%). Adding an aerosol as specified by the fit obtained in section 2, the calculated depolarization values are too low with a median of 3.7% and an IQR of 2.5%. As discussed in section 2, the fit of aerosol parameters is not based on measurements obtained during SHEBA but rather is based on M-PACE measurements, and the concentrations of aerosol in the coarse mode, presumably dominated by sea salt, is expected to be significantly lower during SHEBA than during M-PACE. When we decrease the number concentration in the coarse mode by a factor of 5, the calculated depolarization histogram matches quite well with the observations as seen in Fig. 3, with a median value and IQR of 9.2% and 5.2%, respectively.

Figure 4 shows measured depolarization ratios (from 22:30–23:00 UTC) compared to those calculated based on the *in situ* measured (rather than simulated) size distributions, which are discussed in section 2. For this time span the measured median depolarization is 10%, with an inter-quartile range of 7.9%, similar to the measurements over 22–24 UTC.

When the aerosol distribution with an unscaled coarse mode is included in the lidar calculations, the simulated depolarization ratios compare favorably to the measurements. However, as discussed in section 2, the measured concentration of small ice particles ($D < 200$ μm) likely suffers from ice shattering artifacts. Removing all ice with $D < 200$ μm leads to depolarization ratios that are too low, with a median of 3.9%. When in addition the aerosol coarse mode number concentrations are decreased by a factor 5, the shape of the calculated depolarization distribution as well as the median and IQR, 9.8% and 7.8%, respectively, again compare favorably with the measurements, and are similar to those calculated using the LES output. Aside, we note that removing ice crystals with maximum dimension smaller than 200 μm in the depolarization calculations based on LES output has a neglegible effect (not shown), since very few small ice crystals are found below cloud base in these simulations (Fridlind et al. 2011).

These results show that the low lidar depolarization values can be explained by the presence of ice precipitation and humidified aerosol under cloud base, and that aerosol effects may not generally be negligible under similar conditions, as is often assumed (e.g., Intrieri et al. 2002; van Diedenhoven et al. 2009; de Boer et al. 2011).

5. Conclusion

Measurements by the DABUL lidar below an Arctic stratocumulus layer during the SHEBA campaign in the last 12 hours of May 7th, 1998 show a large range of surprisingly low linear depolarization ratios (4–23%) below cloud base, despite a lack of liquid-phase precipitation. Statistics obtained throughout the SHEBA campaign show that such low

depolarization values are very common (Intrieri et al. 2002). Theoretical depolarization ratios from a range of ice habits typically range from 25–70% (Sassen et al. 1992; Del Guasta et al. 2006; You et al. 2006). Furthermore, the measured depolarization ratios correlate well with radar reflectivity, suggesting that the variation in depolarization ratios results from variations in ice water content, rather than variation in ice habits or orientation. Using simulated lidar measurements based on (i) LES with size-resolved microphysics and (ii) *in situ* ice size distribution measurements, we investigate whether the presence of humidified aerosol can explain the measured distribution of lidar depolarization ratios. Aerosol size distribution measurements are not available for this SHEBA case study, so we follow Morrison et al. (2011) and use aerosol characteristics measured during M-PACE with the total concentration adjusted to reflect the polluted SHEBA conditions. We show that including this aerosol in the lidar calculations leads to an underestimation of the simulated lidar depolarization not only based on LES results but also on *in situ* ice size distributions with small ice crystals ($D < 200$ μm) removed to account for ice shattering effects. Taking into account the fact that SHEBA measurements were obtained above a solid ice pack, while the aerosol size distributions were from marine air sampled during M-PACE, the number concentrations in the aerosol coarse mode were decreased by a factor of 5. With the scaled aerosol coarse mode, the median and IQR of the measured lidar depolarization ratios are very well reproduced by the calculations based on LES output as well as on *in situ* measured ice size distributions.

The uncertainties of the simulated lidar variables presented here are substantial, especially owing to uncertainties in the aerosol size distribution, but also because of limitations of the assumed ice optical properties, LES model assumptions and *in situ* measured ice size distributions. Nevertheless, these results show that humidified aerosols should be taken into

account when interpreting lidar depolarization measurements for cloud and precipitation phase discrimination or for ice habit classification, at least under conditions similar to those observed during SHEBA. Proper aerosol size distribution measurements, and improved ice size distribution measurements, expected to be available from future campaigns in the Arctic, will likely allow to explain the depolarization ratios measured under conditions similar to those explored here in a more comprehensive manner.

Acknowledgments.

This work was supported by the National Aeronautics and Space Administration under Grant No. 06-EOS/06-100 issued through the Science Mission Directorate, Earth Science Division, and by the Department of Energy under Interagency Agreement DE-AI02-06ER64173 issued through the Office of Science, Office of Biological and Environmental Research. MMCR data were obtained from the Atmospheric Radiation Measurement (ARM) Program sponsored by the U.S. Department of Energy, Office of Science, Office of Biological and Environmental Research, Environmental Sciences Division. We thank Paquita Zuidema and Hugh Morisson for their help in obtaining the DABUL data and the *in situ* ice and aerosol size distribution data. Computational resources were provided by the NASA Advanced Supercomputing Division through the NASA High-End Computing Program, and the DOE National Energy Research Scientific Computing Center.

REFERENCES

Ackerman, A. S., O. B. Toon, D. E. Stevens, and J. A. Coakley Jr., 2003: Enhancement of cloud cover and suppression of noctural drizzle in stratocumulus polluted by haze. *Geophys. Res. Lett.*, **30**, 1381, doi:10.1029/2002GL016634.

Beard, K. V., 1992: Ice initiation in warm-base convective clouds: An assessment of microphysical mechanisms. *Atmos. Res.*, **28**, 125–152.

Bourdages, L., T. J. Duck, G. Lesins, J. R. Drummond, and E. W. Eloranta, 2009: Physical properties of high arctic tropospheric particles during winter. *Atm. Chem. Phys.*, **9 (18)**, 6881–6897.

Comstock, K. K., R. Wood, S. E. Yuter, and C. S. Bretherton, 2004: Reflectivity and rain rate in and below drizzling stratocumulus. *Q. J. R. Meteorol. Soc.*, **130**, 2891–2918, doi:10.1256/qj.03.187.

de Boer, G., H. Morrison, M. D. Shupe, and R. Hildner, 2011: Evidence of liquid dependent ice nucleation in high-latitude stratiform clouds from surface remote sensors. *Geophys. Res. Lett.*, **38 (1)**, doi:10.1029/2010GL046016.

Del Guasta, M., E. Vallar, O. Riviere, F. Castagnoli, V. Venturi, and M. Morandi, 2006: Use of polarimetric lidar for the study of oriented ice plates in clouds. *Appl. Opt.*, **45**, 4878–4887.

Fan, J., M. Ovtchinnikov, J. M. Comstock, S. A. McFarlane, and A. Khain, 2009: Ice formation in Arctic mixed-phase clouds: Insights from a 3-D cloud-resolving model with size-resolved aerosol and cloud microphysics. *J. Geophys. Res.*, **114 (D4)**, doi:10.1029/2008JD010782.

Fridlind, A. M., A. S. Ackerman, G. M. McFarquhar, G. Zhang, M. Poellot, P. DeMott, A. Prenni, and A. Heymsfield, 2007: Ice properties of single-layer stratocumulus during the Mixed-Phase Arctic Cloud Experiment: 2. Model results. *J. Geophys. Res.*, **112 (D24)**, D24 202.

Fridlind, A. M., B. van Diedenhoven, A. S. Ackerman, A. Avramov, A. Mrowiec, H. Morrison, P. Zuidema, and M. D. Shupe, 2011: A FIRE-ACE/SHEBA Case Study of Mixed-Phase Arctic Boundary-Layer Clouds: Entrainment Rate Limitations on Rapid Primary Ice Nucleation Processes. *submitted to J . Atmos . Sci .*

Intrieri, J., M. Shupe, T. Uttal, and B. McCarty, 2002: An annual cycle of Arctic cloud characteristics observed by radar and lidar at SHEBA. *J. Geophys. Res.*, **107 (C10)**, 8030, doi:10.1029/2000JC000423.

Korolev, A. and G. Isaac, 2003: Roundness and aspect ratio of particles in ice clouds. *J. Atmos. Sci.*, **60 (15)**, 1795–1808.

Korolev, A. and G. A. Isaac, 2005: Shattering during Sampling by OAPs and HVPS. Part I: Snow Particles. *J. Atm. Ocean. Tech.*, **22 (5)**, 528, doi:10.1175/JTECH1720.1.

Korolev, A. V., E. F. Emery, J. W. Strapp, S. G. Cober, G. A. Isaac, M. Wasey, and D. Marcotte, 2011: Small ice particles in tropospheric clouds: fact or artifact? Airborne

Icing Instrumentation Evaluation Experiment. *Bull. Amer. Meteor. Soc.*, **in press**, doi: 10.1175/2010BAMS3141.1.

Leck, C., M. Norman, E. Bigg, and R. Hillamo, 2002: Chemical composition and sources of the high Arctic aerosol relevant for cloud formation. *J. Geophys. Res.*, **107 (D12)**, doi:10.1029/2001JD001463.

Macke, A., J. Mueller, and E. Raschke, 1996: Single scattering properties of atmospheric ice crystals. *J. Atmos. Sci.*, **53**, 2813–2825.

Mishchenko, M. I. and J. W. Hovenier, 1995: Depolarization of light backscattered by randomly oriented nonspherical particles. *Opt. Lett.*, **20**, 1356–1358.

Mitchell, D. L., 1996: Use of mass- and area-dimensional power laws for determining precipitation particle terminal velocities. *J. Atmos. Sci.*, **53 (12)**, 1710–1723.

Moran, K. P., B. E. Martner, M. J. Post, R. A. Kropfli, D. C. Welsh, and K. B. Widener, 1998: An unattended cloud-profiling radar for use in climate research. *Bull. Amer. Meteor. Soc.*, **79**, 443–455.

Morrison, H., J. O. Pinto, J. A. Curry, and G. M. McFarquhar, 2008: Sensitivity of modeled Arctic mixed-phase stratocumulus to cloud condensation and ice nuclei over regionally varying surface conditions. *J. Geophys. Res.*, **113**, D05 203, doi:10.1029/2007JD008729.

Morrison, H., et al., 2011: Intercomparison of cloud model simulations of arctic mixedphase boundary layer clouds observed during SHEBA. *Submitted to J. Adv. Modeling Earth Systems.*

Noel, V., H. Chepfer, M. Haeffelin, and Y. Morille, 2006: Classification of ice crystal shapes in midlatitude ice clouds from three years of lidar observations over the SIRTA observatory. *J. Atmos. Sci.*, **63**, 2978–2991, doi:10.1175/JAS3767.1.

Noel, V., H. Chepfer, G. Ledanois, A. Delaval, and P. H. Flamant, 2002: Classification of particle effective shape ratios in cirrus clouds based on the lidar depolarization ratio. *Appl. Opt.*, **41**, 4245–4257, doi:10.1364/AO.41.004245.

Sassen, K., H. Zhao, and G. C. Dodd, 1992: Simulated polarization diversity lidar returns from water and precipitating mixed phase clouds. *Appl. Opt.*, **31 (15)**.

Shupe, M. D., 2007: A ground-based multisensor cloud phase classifier. *Geophys. Res. Lett.*, **34 (22)**, doi:10.1029/2007GL031008.

Shupe, M. D., S. Y. Matrosov, and T. Uttal, 2006: Arctic mixed-phase cloud properties derived from surface-based sensors at SHEBA. *J. Atmos. Sci.*, **63**, 697–711, doi:10.1175/JAS3659.1.

Shupe, M. D., T. Uttal, and S. Y. Matrosov, 2005: Arctic cloud microphysics retrievals from surface-based remote sensors at SHEBA. *J. Appl. Met.*, **44 (10)**, 1544–1562, doi:10.1175/JAM2297.1.

Stevens, D. E., A. S. Ackerman, and C. S. Bretherton, 2002: Effects of domain size and numerical resolution on the simulation of shallow cumulus convection. *J. Atmos. Sci.*, **59 (23)**, 3285–3301.

Um, J. and G. M. McFarquhar, 2009: Single-scattering properties of aggregates of plates. *Q. J. R. Meteorol. Soc*, **135 (639)**, 291–304, doi:10.1002/qj.378.

Uttal, T., et al., 2002: Surface heat budget of the arctic ocean. *Bull. Amer. Meteor. Soc.*, **83 (2)**, 255–275.

van Diedenhoven, B., B. Cairns, and P. Yang, 2011: Modeling optical properties of complex ice crystals using equivalent hexagonal columns. *Submitted to J. Appl. Meteor. Climatol.*

van Diedenhoven, B., A. M. Fridlind, A. S. Ackerman, E. W. Eloranta, and G. M. McFarquhar, 2009: An evaluation of ice formation in large-eddy simulations of supercooled Arctic stratocumulus using ground-based lidar and cloud radar. *J. Geophys. Res.*, **114 (D10)**, 1–18, doi:10.1029/2008JD011198.

Weitkamp, C., (Ed.) , 2005: *Lidar, range-resolved optical remote sensing of the atmosphere.* Springer, New York, doi:10.1080/00107510902990209.

Yang, P. and Q. Fu, 2009: Dependence of ice crystal optical properties on particle aspect ratio. *J. Quant. Spectrosc. Radiat. Transfer*, **110**, 1604–1614.

You, Y., G. W. Kattawar, P. Yang, Y. X. Hu, and B. A. Baum, 2006: Sensitivity of depolarized lidar signals to cloud and aerosol particle properties. *J. Quant. Spectrosc. Radiat. Transfer*, **100**, 470–482, doi:10.1016/j.jqsrt.2005.11.058.

Zuidema, P., et al., 2005: An arctic springtime mixed-phase cloudy boundary layer observed during SHEBA. *J. Atmos. Sci.*, **62 (1)**, 160–176, doi:10.1175/JAS-3368.1.

List of Tables

1 Parameters of the bimodal log-normal fit to aerosol measurements 19

TABLE 1. Parameters of the bimodal log-normal fit to aerosol measurements

parameter	Accumulation mode	Coarse mode
r_m [μm]	0.048	0.64
σ_g	2.00	2.62
N [cm^{-3}]	350*	0.9

*Increased from 58 cm^{-3} to represent more polluted conditions during SHEBA.

List of Figures

1 10-minute running means of MMCR radar reflectivity (black, left axis) and lidar linear depolarization ratio (red, right axis) measured during SHEBA in the last 12 hours of 7 May, 1998, averaged below cloud base (140–240 m) of a stratus layer. 21

2 HHPC-6 aerosol size distribution measurements taken during M-PACE, and the bimodal log-normal fit through median values (solid line). The dashed line shows the aerosol distribution with the number concentration increased in accumulation mode to represent polluted SHEBA conditions. The dotted line shows the fit of Morrison et al. (2008). 22

3 Histograms of measured lidar depolarization ratios over 22–24 UTC (yellow), and those calculated based on the LES output, including no humidified aerosol (black), including all humidified aerosol (blue) and including humidified aerosol with the number concentration in the coarse mode decreased by a factor 5 (red). 23

4 Histograms of measured lidar depolarization ratios over 22:30–23:00 UTC (yellow) , and those calculated based on the in situ measured ice size distributions, when all humidified aerosol and all ice is included (black), when all humidified aerosol and only large ice is included (blue), and when only large ice and humidified aerosol with the number concentration in the coarse mode decreased by a factor 5 is included (red). 24

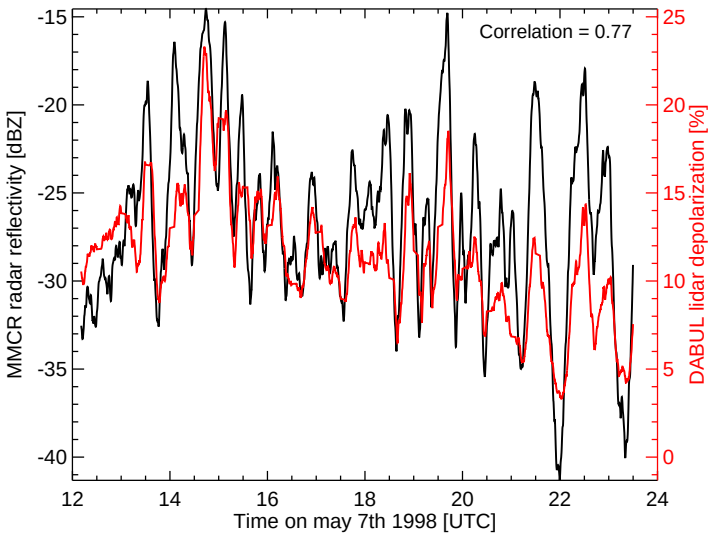

FIG. 1. 10-minute running means of MMCR radar reflectivity (black, left axis) and lidar linear depolarization ratio (red, right axis) measured during SHEBA in the last 12 hours of 7 May, 1998, averaged below cloud base (140–240 m) of a stratus layer.

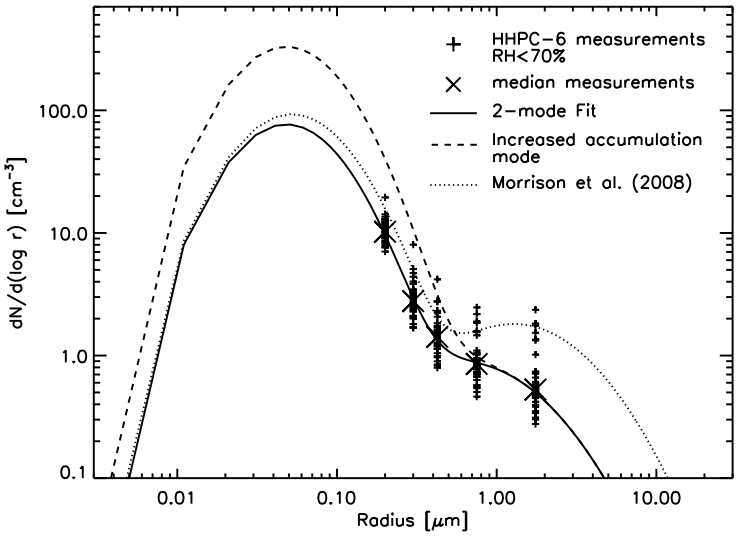

FIG. 2. HHPC-6 aerosol size distribution measurements taken during M-PACE, and the bimodal log-normal fit through median values (solid line). The dashed line shows the aerosol distribution with the number concentration increased in accumulation mode to represent polluted SHEBA conditions. The dotted line shows the fit of Morrison et al. (2008).

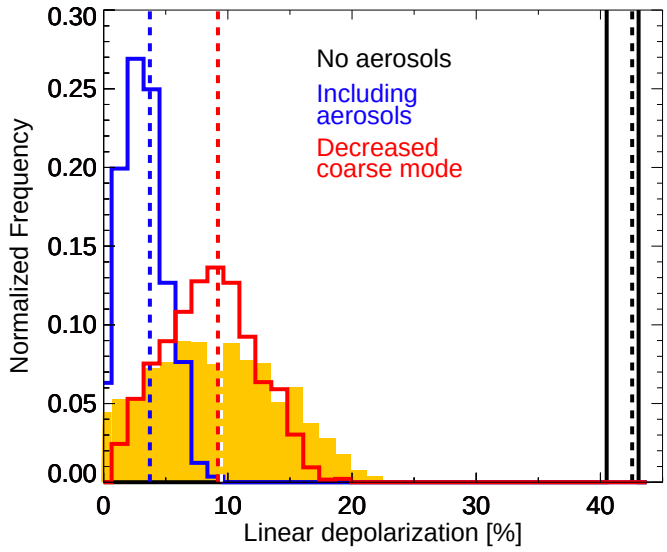

FIG. 3. Histograms of measured lidar depolarization ratios over 22–24 UTC (yellow), and those calculated based on the LES output, including no humidified aerosol (black), including all humidified aerosol (blue) and including humidified aerosol with the number concentration in the coarse mode decreased by a factor 5 (red).

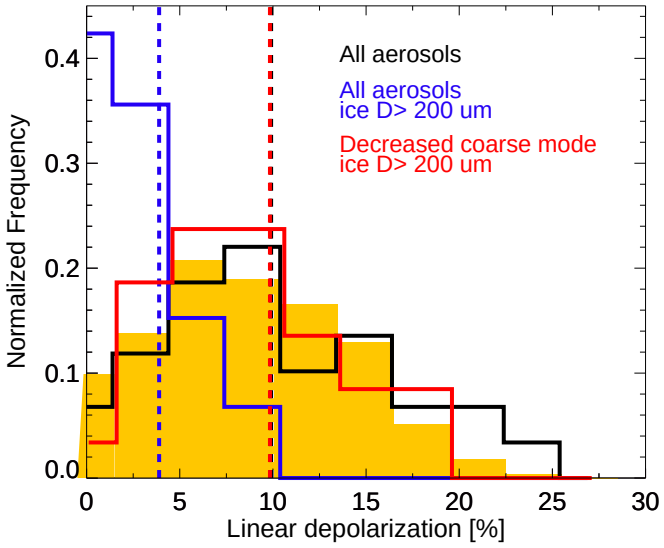

FIG. 4. Histograms of measured lidar depolarization ratios over 22:30–23:00 UTC (yellow) , and those calculated based on the in situ measured ice size distributions, when all humidified aerosol and all ice is included (black), when all humidified aerosol and only large ice is included (blue), and when only large ice and humidified aerosol with the number concentration in the coarse mode decreased by a factor 5 is included (red).